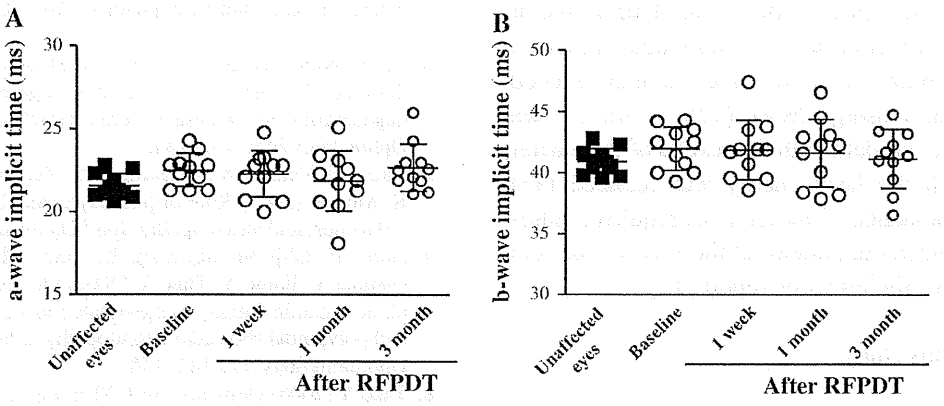

Fig. 6 Averaged implicit times of the focal macular electroretinograms (ERG) a- (**a**) and b-waves (**b**). *Circles* represent eyes affected by polypoidal choroidal vasculopathy before and after reduced fluence photodynamic therapy (RFPDT). *Filled squares* represent unaffected eyes of the patients. *Error bars*: mean ± SD

A recurrence of exudative changes including a SRD and subretinal hemorrhage was seen in 4 eyes (27%) over the 12-month follow-up period. These complications required additional treatments, and the averaged number of treatments was 1.4 over the one-year observation period. Nine of the 11 eyes (82%) had a recurrence during the observation period with a mean of 26 months and ranging from 13 to 34 months.

Small subretinal hemorrhages less than 1/4 disk diameter were seen in 2 patients within the 1-month postoperative period (18%). A transient increase in an SRD was seen in one patient at 1 week after the treatment (9%).

Discussion

Our results showed that RFPDT improved the visual acuity and reduced the thickness of the fovea. It had no adverse effects on the macula function and choroidal circulation in our patients with PCV.

Preservation of focal macular ERGs

Earlier studies that evaluated the macular function by focal macular ERGs demonstrated a significant reduction in the amplitudes of the focal macular ERGs following the standard PDT procedures [10, 11]. Choroidal circulatory disturbances and/or inflammatory responses associated with vascular leakage may have contributed to these alterations.

Ishikawa et al. [10, 16] reported a significant correlation between choroidal hypoperfusion induced by the standard PDT and the decreased amplitudes of the focal macular ERGs. In cases with choroidal hypoperfusion, the amplitudes of the a- and b-waves of the focal macular ERGs were significantly reduced at both 1 week and 1 month postoperatively. A choroidal hypoperfusion did not develop after RFPDT in any of our patients. In addition, the foveal thickness was significantly reduced at 1 week after RFPDT indicating that the vascular leakage associated with the inflammatory reaction most likely did not develop. These two factors possibly contributed to the retention of the macular function following RFPDT.

Although a functional recovery has been reported at 3 months after the standard PDT, there was no improvement in the amplitudes of the focal macular ERGs [10]. We found a significant increase in the b-wave amplitudes at 3 months after the RFPDT. This suggests that RFPDT as opposed to standard PDT could enhance the early improvement of macular function.

Comparison of our results with those using standard PDT

Earlier studies have shown that the standard PDT is more effective for eyes with PCV than eyes with typical AMD [6–8]. However, in long-term observations, recurrences of the exudative changes have been seen in approximately 60% within 2 years and 80% within 3 years after standard PDT [17, 18]. The recurrence rate in our patients was 82% after 26 months indicating that RFPDT did not reduce the recurrence rate significantly from that of standard PDT.

We reduced the exposure time to one-half of that of the standard protocol because earlier studies reported that a reduced time was more effective than reduced laser energy in closing CNVs [12]. However, we cannot compare our data with the results of the earlier report in which the laser energy was reduced [13] although the incidence of recurrences requiring additional treatments in our patients at the 1 year time was similar to that of the previous report [13].

Limitation of this study

One important limitation of this study was the lack of control patients treated with standard PDT. Therefore, we compared our data with those reported in which the AMD and PCV patients were treated with the standard PDT and the macular function was evaluated by the focal macular ERGs using very similar recording systems to ours [10]. However, our patients were selected to have relatively small PCV lesions that might well respond to the treatments. In addition, the sample size was too small to determine the long-term benefits of RFPDT. Further studies including larger numbers of patients with various size lesions are needed to determine the long-term benefit of RFPDT for PCV.

Acknowledgments This work is supported by Grant-in-Aid for Scientific Research C from Ministry of Education, Science and Culture in Japan No. 20592056.

Conflict of interest None.

References

1. Yannuzzi LA, Sorenson J, Spaide RF, Lipson B (1990) Idiopathic polypoidal choroidopathy (IPCV). Retina 10:1–8
2. Spaide RF, Yannuzzi LA, Slakter JS, Sorenson J, Orlach DA (1995) Indocyanine green videoangiography of idiopathic polypoidal choroidal vasculopathy. Retina 15:100–110
3. Sho K, Takahashi K, Yamada H, Wada M, Nagai Y, Otsuji T, Nishikawa M, Mitsuma Y, Yamazaki Y, Matsumura M, Uyama M (2003) Polypoidal choroidal vasculopathy: incidence, demographic features, and clinical characteristics. Arch Ophthalmol 121:1392–1396
4. Maruko I, Iida T, Saito M, Nagayama D, Saito K (2007) Clinical characteristics of exudative age-related macular degeneration in Japanese patients. Am J Ophthalmol 144: 15–22
5. Liu Y, Wen F, Huang S, Luo G, Yan H, Sun Z, Wu D (2007) Subtype lesions of neovascular age-related macular degeneration in Chinese patients. Graefes Arch Clin Exp Ophthalmol 245:1441–1445
6. Akaza E, Yuzawa M, Matsumoto Y, Kashiwakura S, Fujita K, Mori R (2007) Role of photodynamic therapy in polypoidal choroidal vasculopathy. Jpn J Ophthalmol 51:270–277
7. Gomi F, Ohji M, Sayanagi K, Sawa M, Sakaguchi H, Oshima Y, Ikuno Y, Tano Y (2008) One-year outcomes of photodynamic therapy in age-related macular degeneration and polypoidal choroidal vasculopathy in Japanese patients. Ophthalmology 115:141–146
8. Tano Y (2008) Guideline for PDT in Japan. Ophthalmology 115:585
9. Treatment of age-related macular degeneration with photodynamic therapy (TAP) study group, verteporfin in photodynamic therapy (VIP) study group (2004) Acute severe visual acuity decrease after photodynamic therapy with verteporfin: case reports from randomized clinical trials—TAP and VIP report No. 3. Am J Ophthalmol 137:683–696
10. Ishikawa K, Kondo M, Ito Y, Kikuchi M, Nishihara H, Piao CH, Sugita T, Terasaki H (2007) Correlation between focal macular electroretinograms and angiographic findings after photodynamic therapy. Invest Ophthalmol Vis Sci 48: 2254–2259
11. Lai TYY, Chan WM, Lam DSC (2004) Transient reduction in retinal function revealed by multifocal electroretinogram after photodynamic therapy. Am J Ophthalmol 137:826–833
12. Michels S, Hansmann F, Geitzenauer W, Schmidt-Erfurth U (2006) Influence of treatment parameters on selectivity of verteporfin therapy. Invest Ophthalmol Vis Sci 47:371–376
13. Yamashita A, Shiraga F, Shiragami C, Ono A, Tenkumo K (2010) One-year results of reduced-fluence photodynamic therapy for polypoidal choroidal vasculopathy. Am J Ophthalmol 149:465–471
14. Japanese Study Group of Polypoidal Choroidal Vasculopathy (2005) Criteria for diagnosis of polypoidal choroidal vasculopathy. J Jpn Ophthalmol Soc 109:417–427
15. Miyake Y, Yanagida K, Kondo K, Ota I (1981) Subjective scotometry and recording of local electroretinogram and visual evoked response. System with television monitor of the fundus. Jpn J Ophthalmol 25:439–448
16. Ishikawa K, Nishihara H, Ozawa S, Piao CH, Ito Y, Kondo M, Terasaki H (2009) Focal macular electroretinograms after photodynamic therapy combined with posterior juxtascleral triamcinolone acetonide. Retina 29:803–810
17. Akaza E, Mori R, Yuzawa M (2008) Long-term results of photodynamic therapy of polypoidal choroidal vasculopathy. Retina 28:717–722
18. Akaza E, Yuzawa M, Mori R (2011) Three-year follow-up results of photodynamic therapy for polypoidal choroidal vasculopathy. Jpn J Ophthalmol 55:39–44

Clinical Ophthalmology

Dovepress

CASE REPORT

Choroidal findings in idiopathic uveal effusion syndrome

Tomomi Harada
Shigeki Machida
Takamistu Fujiwara
Yasunori Nishida
Dajiro Kurosaka

Department of Ophthalmology, Iwate Medical University School of Medicine, Iwate, Japan

Purpose: We report choroidal findings by means of enhanced depth imaging spectral-domain optical coherence tomography (EDI-OCT) in a patient with idiopathic uveal effusion syndrome (IUES).

Case report: A 41-year-old man was referred to us with ciliochoroidal and non-rhegmatogenous retinal detachments. Sclerectomies and sclerostomies were performed at the equator in the lower quadrants, resulting in resolution of the ciliochoroidal and retinal detachments. EDI-OCT demonstrated low-reflective areas in the outer choroid. The subfoveal choroidal thickness measured vertically from the outer border of the RPE to the inner border of the sclera was 787 μm which was significantly thicker than the normal value (272 ± 90 μm, n = 131) obtained from age-matched normal controls.

Conclusions: The findings made by EDI-OCT have provided additional evidence that choroidal alterations play a role in the pathological process in IUES.

Keywords: uveal effusion syndrome, spectral-domain optical coherence tomography, EDI-OCT, OCT, choroid

Introduction

Idiopathic uveal effusion syndrome (IUES) is a rare disease characterized by ciliochoroidal and non-rhegmatogenous retinal detachments associated with an abnormality of trans-scleral diffusion of extravascular proteins in the choroid.[1,2] Therefore, enhancement of protein diffusion by lamellar sclerectomies and sclerostomies results in resolution of the ciliochoroidal and non-rhegmatogenous retinal detachments.[3]

Enhanced depth imaging spectral-domain optical coherence tomography (EDI-OCT) has been developed to allow clinicians to evaluate the thickness and structure of the choroid.[4] For example, it has been demonstrated in EDI-OCT images that choroidal thickness is significantly thinner in highly myopic eyes.[5]

We present our EDI-OCT findings together with the choroidal angiographic findings in a patient with IUES.

Case report

A 41-year-old man was referred to us in July 2001 complaining of decreased vision in his right eye. He had a history of serous macular detachments in both eyes in 1996, which resolved spontaneously. Otherwise, he was healthy. His best-corrected visual acuity (BCVA) was 0.3 OD and 1.0 OS with mild myopia in both eyes. The intraocular pressures were normal. The axial lengths of the globe were 22.95 mm and 22.65 mm for the right and left eyes, respectively. There were no inflammatory cells in the anterior

Correspondence: Shigeki Machida
Department of Ophthalmology, Iwate Medical University, School of Medicine, 19-1 Uchimaru Morioka Iwate 020-8505, Japan
Tel +81 19 651 5111 (ext 8691)
Fax +81 19 653 2864
Email smachida@iwate-med.ac.jp

chamber and vitreous cavity in either eyes. The posterior pole of the ocular fundus showed atrophy of the retinal pigment epithelium (RPE; Figure 1A). An annular ciliochoroidal detachment and a shifting bullous retinal detachment were noted in the right eye (Figure 1B and C). In the left eye, a ciliochoroidal detachment was seen in the temporal hemisphere without retinal detachment. The vortex veins were only discernible in the temporal superior quadrant in the right eye and in the inferior lower quadrant in the left eye.

Sclerectomies and sclerostomies were performed at the equator in the lower quadrants of the right eye in September 2001, resulting in resolution of the ciliochoroidal and retinal detachments. During the surgery, we noted that the sclera was rigid and thick. The ciliochoroidal and retinal detachments recurred 6 months after the surgery, and the vision decreased to light perception in the right eye because of chorioretinal atrophy.

The patient re-visited us complaining of decreased vision in the left eye, in September 2005. The BCVA was light perception OD and 0.3 OS. Atrophy of the RPE in the posterior pole and annular ciliochoroidal detachments were noted in the left eye (Figure 1D and E). OCT demonstrated subretinal fluid in the macula (Figure 1F). We performed sclerectomies and sclerostomies with application of mitomycin C (MMC) in the inferior quadrants of the left eye in November 2005. Medical Quick Absorber® (Inami Co, Tokyo, Japan) soaked in 0.04% MMC was placed on the sclera after the sclerostomies for 5 minutes to avoid postoperative fibrosis as used for glaucoma filtering surgery. The ciliochoroidal and retinal detachments promptly resolved after surgery with improvement of vision to 1.0.

The patient returned because of a relapse in the left eye in March 2010. His BCVA had deteriorated to 0.7 OS. OCT demonstrated a serous macular detachment and intraretinal fluid.

In May 2010, fluorescein angiography (FAG) showed marked hyperfluorescence in the macular region of the left eye due to window defect with late subretinal leakage (Figure 2A and B). Indocyanine green angiography (ICGA) revealed diffuse and moderate hyperfluorescence that obscured large choroidal veins in the posterior pole of the ocular fundus in the early phase (Figure 2C), which was consistent with previously reported ICGA findings.[6] In the late phase of ICGA, hypofluorescence was noted throughout the posterior pole (Figure 2D). Topical steroid application resulted in a resolution of the serous macular detachment and the intraretinal fluid in the left eye, with improvement in vision.

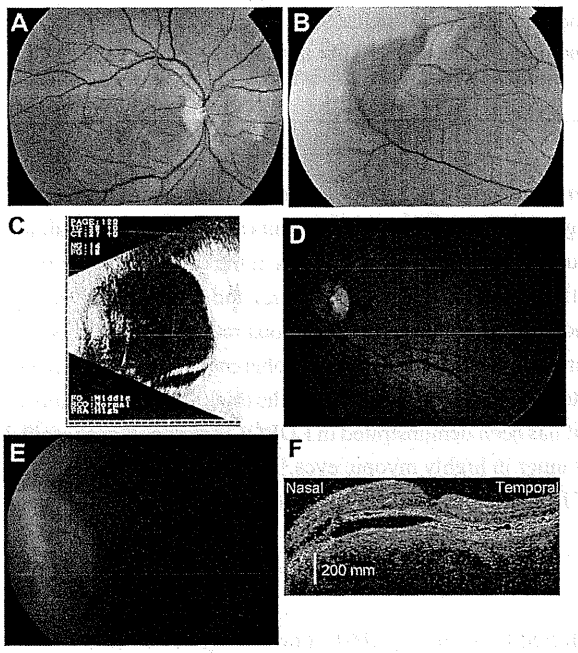

Figure 1 Photograph of the posterior pole (A) and peripheral region (B) of the right eye of a patient with idiopathic uveal effusion syndrome (IUES) in July 2001. A choroidal detachment can be seen (B). The ultrasonographic image of the right eye shows a retinal detachment in the inferior hemisphere (C). Photograph of the posterior pole (D) and peripheral region (E) of the left eye in September 2006. A ciliochoroidal detachment can be seen (E). Optical coherence tomography shows a macular detachment in the left eye (F).

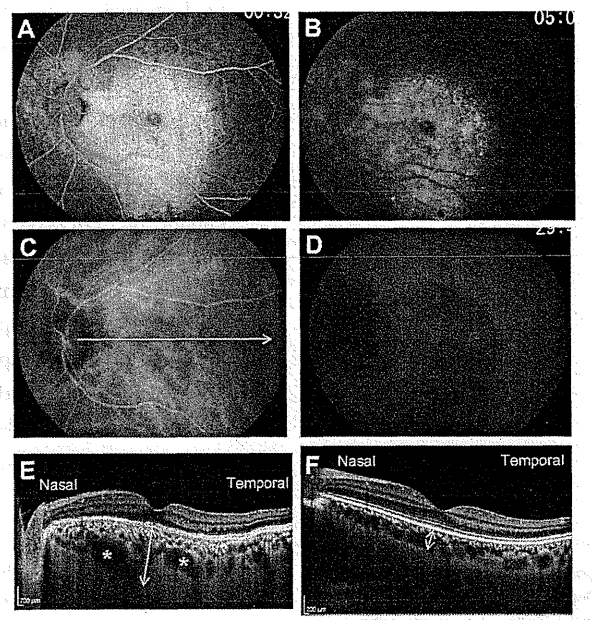

Figure 2 Fluorescein angiograms (A and B) and indocyanine green angiograms (C and D) in May 2008. The arrow points to the direction and length of the enhanced depth imaging optical coherence tomographic scan (EDI-OCT) (C). The EDI-OCT image shows large low-reflective areas (indicated by asterisks) in the outer choroid in the patient (E) which was not noted in a control subject (F).

The arrow and line in Figure 2C indicates the direction and length of the EDI-OCT scan. EDI-OCT demonstrated low-reflective areas (indicated by asterisks in Figure 2E) in the outer choroid (Figure 2C and E) in April 2011. The subfoveal choroidal thickness was measured vertically from the outer border of the RPE to the inner border of the sclera. The choroidal thickness was 787 μm (indicated by the arrow in Figure 2E) which was significantly thicker than the normal value (272 ± 90 μm, n = 131) obtained from age-matched normal controls (indicated by the arrow in Figure 2F).

Discussion

Our patient had annular ciliochoroidal detachments with shifting subretinal fluid which was resolved by the sclerectomies and sclerostomies. The patient was a healthy and middle-aged man without nanophthalmos or medical history of any other disease. These characteristics are consistent with those of IUES.[2]

The EDI-OCT images showed large low-reflective areas in the outer choroid, which could represent dilated choroidal veins or an enlargement of the suprachoroidal space. The ICGA failed to delineate large choroidal veins in the posterior pole in the early phase because of the diffuse hyperfluorescence throughout the ocular fundus. However, congestion of the choroidal veins could take place because of the abnormality of the vortex veins. Alternatively, the low-reflective areas in the EDI-OCT images may represent an accumulation of extravascular proteins in the suprachoroidal space. These choroidal findings are comparable to the hypothesized disease mechanism of IUES in which extravascular proteins triggered by choroidal congestion accumulate in the suprachoroidal space leading to choroidal and retinal detachments.[3] A congenital anomaly of the sclera superimposed on aging and hormonal changes is hypothesized to prevent transport of extravascular proteins across the sclera.[3] In fact, the sclera of our patient appeared to be thick and rigid during the surgeries.

The findings made by EDI-OCT have provided additional evidence that choroidal alterations play a role in the pathological process in IUES.

Disclosure

The authors report no conflicts of interest in this work.

References

1. Schepens CL, Brockhurst RJ. Uveal effusion. I. Clinical picture. *Arch Ophthalmol*. 1963;70:189–201.
2. Gass JDM, Jallow S. Idiopathic serous detachment of the choroid, ciliary body, and retina (uveal effusion syndrome). *Ophthalmology*. 1982;89(9):1018–1032.
3. Gass JDM. Uveal effusion syndrome. A new hypothesis concerning pathogenesis and technique of surgical treatment. *Retina*. 1983;3(3) 159–163.
4. Spaide RF, Koizumi H, Pozonni MC. Enhanced depth imaging spectral-domain optical coherence tomography. *Am J Ophthalmol*. 2008;146(4):496–500.
5. Fujiwara T, Imamura Y, Margolis R, Slakter JS, Spaide RF. Enhanced depth imaging optical coherence tomography of the choroid in highly myopic eyes. *Am J Ophthalmol* 2009;148(3):445–450.
6. Uyama M, Takahashi K, Kozaki J, et al. Uveal effusion syndrome: clinical features, surgical treatment, histologic examination of the sclera, and pathophysiology. *Ophthalmology*. 2000;107(3).441–449.

Enhancement of ON-Bipolar Cell Responses of Cone Electroretinograms in Rabbits with the Pro347Leu Rhodopsin Mutation

Tomoharu Nishimura,[1] *Shigeki Machida,*[1] *Mineo Kondo,*[2,3] *Hiroko Terasaki,*[2] *Daisuke Yokoyama,*[1] *and Daijiro Kurosaka*[1]

Purpose. To determine how the different stages of retinal processing change after photoreceptor degeneration in rabbits carrying the Pro347Leu rhodopsin mutation (Tg rabbits).

Methods. Cone electroretinograms (ERGs) were elicited by 150-ms duration stimuli from 13 Tg rabbits at 12 and 24 weeks of age. The ERG recordings were made before and after an intravitreal injection of tetrodotoxin citrate (TTX) plus *N*-methyl-DL-aspartic acid (NMDA), with the addition of 2-amino-4-phosphonobutyric acid (APB) and then *cis*-2,3-piperidine-dicarboxylic acid (PDA) or 6-cyano-7-nitroquinoxaline-2,3-dione (CNQX). Digital subtraction of the ERG after the injection from the ERG before the injection was used to extract the components that were blocked by these drugs. Thirteen age-matched, wild-type (WT) rabbits were studied with the same protocol.

Results. In Tg rabbits, the cone ERGs elicited by intermediate intensities had a depolarizing pattern. At 12 weeks of age, the photoreceptor and OFF-bipolar/horizontal cell responses reflected in the ERG in the Tg rabbits did not differ significantly from those in the WT rabbits. The ON-bipolar cells and the third-order neuronal responses recorded after pharmacologic blockade were significantly enhanced in the Tg rabbits compared with those recorded in the WT rabbits. At 24 weeks of age, the ERG waveforms representing the photoreceptors and OFF-bipolar/horizontal cell responses were significantly decreased, but those representing the ON-bipolar cell and third-order neuronal responses were still preserved in the Tg rabbits.

Conclusions. A depolarizing pattern of the cone ERG responses was seen in Pro347Leu Tg rabbits. The enhancement or preservation of the ON-bipolar cell response in the ERGs contributed to shaping the waveform in the Tg rabbits. In this model, the functional alterations in the ON-pathway took place before the deterioration of cone photoreceptor function. (*Invest Ophthalmol Vis Sci.* 2011;52:7610–7617) DOI:10.1167/iovs.11-7611

From the [1]Department of Ophthalmology, Iwate Medical University School of Medicine, Iwate, Japan, the [2]Department of Ophthalmology, Nagoya University Graduate School of Medicine, Aichi, Japan.

[3]Present affiliation: Department of Ophthalmology, Mie University Graduate School of Medicine, Mie, Japan.

Supported by Grant-in-Aid for Scientific Research C 20592056 (SM) from the Ministry of Education, Science, and Culture in Japan; and the Japanese Retinitis Pigmentosa Society (JRPS).

Submitted for publication March 23, 2011; revised July 4 and August 9, 2011; accepted August 13, 2011.

Disclosure: **T. Nishimura**, None; **S. Machida**, None; **M. Kondo**, None; **H. Terasaki**, None; **D. Yokoyama**, None; **D. Kurosaka**, None

Corresponding author: Shigeki Machida, Department of Ophthalmology, Iwate Medical University, School of Medicine, 19-1 Uchimaru Morioka Iwate 020-8505, Japan; smachida@iwate-med.ac jp.

The retinal degeneration in eyes with retinitis pigmentosa (RP) is caused by mutations of different genes related to the photoreceptors and retinal pigment epithelium. Rhodopsin is a photosensitive molecule that is expressed in the photoreceptor, and more than 100 distinct mutations of the rhodopsin gene have been found to be associated with autosomal dominant retinitis pigmentosa (adRP) (http://www.sph.uth.tmc.edu/RetNet/; provided by the University of Texas Houston Health Science Center, Houston, TX).[1–3] Among these, mutations near the carboxyl terminus of the rhodopsin gene (e g., Pro347Leu) are associated with poorer visual outcome than those near the amino terminus (e.g., Pro23His).[4,5]

Animal models are used to acquire information on the pathophysiology of diseases and to develop new treatments. Most of the animal models of adRP are murine models that have progressive photoreceptor degeneration similar to that in human adRP.[6–9] However, the small size of the murine eyes makes it difficult to perform surgery and other procedures on them and has led to the development of larger animal models of adRP

Peng et al.[10] created transgenic swine with the Pro347Leu rhodopsin mutation. More recently, Kondo et al.[11] created transgenic rabbits carrying the Pro347Leu rhodopsin mutation (Tg), and these rabbits were shown to have a progressive loss of photoreceptors. Kondo et al. used the electroretinogram (ERG) to demonstrate that the rod function was lost before cone function in Tg rabbits. This effect is similar to the course of the functional changes in humans with adRP. Because rabbits have large eyes, multiple intravitreal injections of drugs, implantation of retinal prostheses, and cell-based therapy can be performed on them.

The intravitreal injection of drugs (e g., glutamate analogues) that block specific receptors on the retinal neurons has been used to determine the contribution of different retinal neurons to the ERGs. For example, Sakai et al.[12] showed that an intravitreal injection of tetrodotoxin (TTX), which blocks the voltage-gated sodium channels of the retinal ganglion cells (RGCs) and amacrine cells,[13–15] eliminated the enhanced OPs in young Tg rabbits In addition, our laboratory has shown that the ON-bipolar cell contribution to the multifocal ERGs (mfERGs) was significantly enhanced in Tg rabbits at the early stage of retinal degeneration.[16] These results, obtained by pharmacologic dissection of the retinal circuits, showed that the inner and middle retinal responses were altered in the early stage of photoreceptor degeneration in Tg rabbits.

Cone ERGs are dominated by contributions from ON- and OFF-bipolar cells. An imbalance between the ON- and OFF-bipolar cell responses and the presence or absence of horizontal feedback to the cones results in cone ERGs with either a depolarizing or a hyperpolarizing pattern.[17,18]

We compared the waveform of the cone ERGs of Tg rabbits to those of WT rabbits and showed that the cone ERGs of the Tg

rabbits have a depolarizing pattern. We also used pharmacologic agents to dissect the cone ERGs elicited by long-duration stimuli to investigate how the different types of retinal neurons contribute to the depolarizing pattern of the ERGs in Tg rabbits.

Methods

Animals

We used heterozygous Pro347Leu rhodopsin Tg rabbits, line 7, which have the highest level of transgene expression and the most severe photoreceptor degeneration.[11] Thirteen 10-week-old Tg New Zealand albino rabbits were purchased from Kitayama Laboratories Co., Ltd. (Nagano, Japan) and kept in the animal colony until the experiments. Thirteen wild-type (WT) New Zealand albino rabbits were used as controls. The experiments were performed on different sets of rabbits at 12 and 24 weeks of age.

All animals were housed and handled under the authorization and supervision of the Institutional Animal Care and Use Committee of the Iwate Medical University. All the procedures involving the rabbits conformed to the ARVO Statement for the Use of Animals in Ophthalmic and Vision Research.

ERG Recordings

The rabbits were anesthetized with a loading dose of intramuscular xylazine (2 mg/kg) and ketamine (25 mg/kg), and anesthesia was maintained by hourly injection of a mixture of xylazine (1 mg/kg) and ketamine (13 mg/kg). The pupils were maximally dilated with a mixture of 0.5% tropicamide and 0.5% phenylephrine HCl applied topically.

After the cornea was anesthetized by topical oxybuprocaine, a contact lens electrode containing light-emitting diodes (LEDs, EW-102; Mayo, Nagoya, Japan) was inserted. The LEDs provided homogenous white (color temperature, 4000–9000 K) stimuli and background illumination. The luminance was measured at the corneal surface with a photometer (model LS-100; Minolta, Tokyo, Japan). The characteristics of the contact lens electrode have been described in detail.[19] A needle reference electrode was inserted subcutaneously into the forehead, and the ground electrode was placed on the right ear lobe.

The cone ERGs were elicited by stimuli of 150-ms duration presented on a diffuse white background of 40 cd/m^2. The animals were light-adapted by the white background light of 40 cd/m^2 for at least 10 minutes before the cone ERG recordings. The ERGs were amplified 5000× and band-pass filtered from 0.5 to 1000 Hz (Neuropack MED 5210; Nihon Kohden, Tokyo, Japan). The stimulus intensity ranged from 1.5 to 3.5 log cd/m^2 with increments of 0.2-, 0.3-, or 0.5-log unit steps. The intensity and duration of the stimuli were controlled by an electronic function generator (model WLS-20; Mayo) connected to the LEDs.

Drug Injections

TTX (Latoxan, Valence, France), *N*-methyl-D-aspartic acid (NMDA), 2-amino-4-phosphonobutyric acid (APB), and *cis*-2, 3-piperidine-dicarboxylic acid (PDA) were purchased from Sigma-Aldrich (St. Louis, MO) and were injected into the vitreous cavity of the Tg and WT rabbits. Each of these drugs blocked the activity of a specific type of retinal neuron, which then allowed us to determine the neuron's contribution to the ERGs.

First, TTX+NMDA were injected into the vitreous. TTX blocks voltage-gated sodium channels and thus blocks action potentials produced by RGCs and spiking amacrine cells.[13–15] NMDA depolarizes the different types of amacrine cells and most RGCs,[20] rendering them unresponsive to light stimuli. Therefore, the third-order neuronal responses should have been largely eliminated after an intravitreal injection of TTX+NMDA.[21]

Second, APB was injected intravitreally. APB is an agonist of metabotropic glutamate receptor type 6 (mGluR6) and blocks the synaptic transmission between the photoreceptors and ON-bipolar cells.[22] Finally, we injected PDA which is an antagonist of AMPA/KA class ionotropic glutamate receptors (iGluR) and blocks the light responses of OFF-bipolar cells, horizontal cells, and many amacrine and RGCs.[23] Because PDA is not commercially available, 6-cyano-7-nitroquinoxaline-2,3-dione (CNQX), which has effects similar to those of PDA on retinal neural cells and ERGs, was used in some of the experiments.[24,25]

Each drug was dissolved in normal saline, and the pH was adjusted to 6.8 to 7.2 with 1 N NaOH. Then, a 30-gauge needle attached to a 1-mL syringe was inserted 3.5 mm posterior to the corneal limbus into the midvitreous, and 0.04 mL of the solution was injected. The estimated concentration of each solution was 4 μM for TTX; 5 mM for NMDA, APB, and PDA; and 200 μM for CNQX, assuming a complete mixing in the 1.2-mL vitreous of rabbits.[26] These estimated concentrations of the drugs were determined according to earlier studies in rabbits and primates.[12,18,21,27,28] The ERG recordings were made between 60 and 90 minutes after the intravitreal injection of each pharmacologic agent or agent combination.

Statistic Analyses

A two-way repeated-measures ANOVA was used to compare the intensity–response curves of the WT rabbits to those of the Tg rabbits. In addition, two-tailed Student's *t* tests were used to determine the statistical significance of differences in the amplitudes at each stimulus intensity between the WT and the Tg rabbits. The level of statistical significance was set at $P < 0.05$ (Prism 5.1; GraphPad Software Inc., San Diego, CA).

Results

Cone ERGs of Tg and WT Rabbits Elicited by Long-Duration Stimuli

All ERG waveforms in this article represent the averaged ERGs recorded from three or five animals. For example, the ERGS shown in Figure 1A were recorded at a stimulus intensity of 3.0 log cd/m^2 in five WT rabbits and then averaged (represented by the thick line).

The cone ERGs elicited by long-duration stimuli from the 12- and 24-week-old Tg (red lines) and WT (black lines) rabbits are shown in Figure 1B. The ERGs shown are the averages of five animals. At 12 weeks of age, there was no difference between the Tg and WT rabbits in the amplitudes and implicit times of the b-wave for all stimulus intensities. However, in the intermediate stimulus range between 2.0 and 3.0 log cd/m^2, the potential level after the b-wave peak remained elevated and did not return to the baseline until the stimulus was turned off in the Tg rabbits. The waveform in the Tg rabbits seen in this intermediate stimulus range had a depolarizing pattern. On the other hand, the potential level after the b-wave rapidly returned to baseline level in the WT rabbits. The waveforms of the Tg rabbits at the lowest and highest intensities did not differ noticeably from those of the WT rabbits. In the Tg rabbits 24 weeks of age, a depolarizing pattern was also seen at the intermediate stimulus intensities.

Waveform Changes in Cone ERGs after Intravitreal Drug Injections

The changes in the shape of the ERGs of the 12-week-old WT rabbits after each drug injection at a stimulus intensity of 3.0 log cd/m^2 are shown in Figure 2A. The ERG waveforms of five animals were averaged. After the intravitreal injections of TTX and NMDA (post-TTX+NMDA), the ERG waveforms became more positive and square shaped with a loss of the oscillatory potentials.

Then, APB was injected intravitreally to block synaptic transmission between the photoreceptors and ON-bipolar cells. After the injection of APB, the b-wave disappeared and the ERG had a negative shape, which was derived from activity

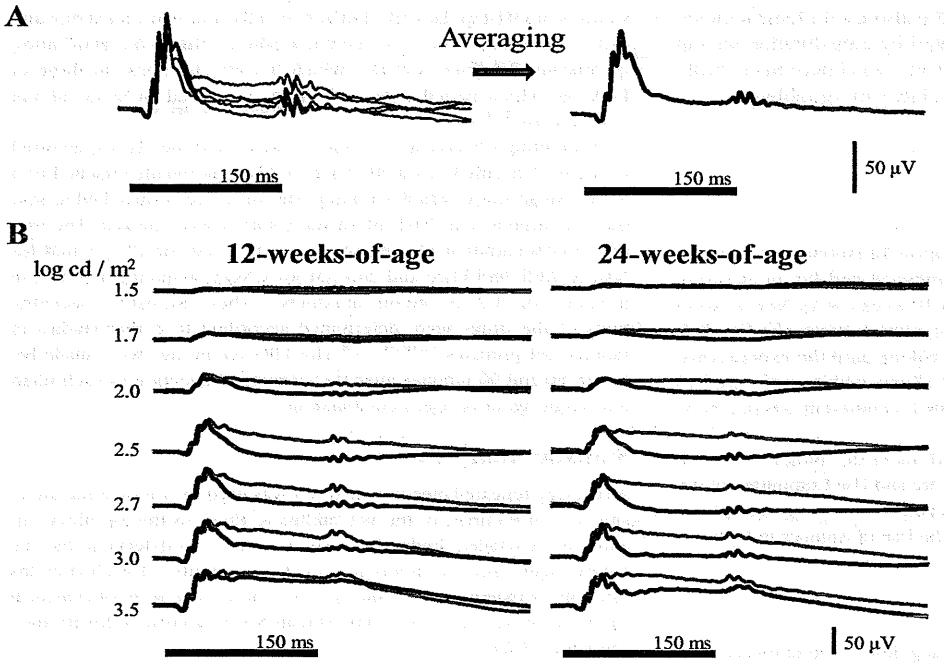

FIGURE 1. (A) Averaged ERG waveforms recorded from five individual rabbits. (B) Averaged waveforms of ERGs recorded from the Pro347Leu Tg (n = 5) and WT (n = 5) rabbits at 12 and 24 weeks of age. *Black* and *red lines*: ERGs recorded from the WT and Tg rabbits, respectively.

of cone photoreceptors and OFF-bipolar/horizontal cells (post-TTX+NMDA+APB). Finally, PDA was injected to eliminate responses from OFF-bipolar/horizontal cells, leaving a small, slow, negative response originating from the cone photoreceptors (post-TTX+NMDA+APB+PDA).

Isolation of Responses from Each Type of Retinal Neuron

Digital subtraction of the ERG waveforms extracted the components that were blocked by the drugs. Therefore, by subtracting the post-TTX+NMDA ERGs from the pre-TTX+NMDA ERGs (baseline waveforms), the response of the third-order neurons could be isolated (Fig. 2, A minus B). By subtracting post-TTX+NMDA+APB from the post-TTX+NMDA waveform, the ON-bipolar cell response was isolated (Fig. 2, B minus C). Finally, we subtracted the post-TTX+NMDA+APB+PDA from the post-TTX+NMDA+APB to isolate the OFF-bipolar/horizontal cell response (Fig. 2, C minus D).

The isolated responses consisted of slow waves, which made it difficult to determine a peak of each wave. Therefore, we measured the amplitude at 75 ms after the light onset (midway between onset and offset). The mean amplitudes with the standard deviations are plotted against the stimulus intensities in Figures 3 to 7.

Intensity–Response Curves of Pharmacologically Isolated Responses

The averaged isolated cone photoreceptor responses of the Tg rabbits were very similar to those of the WT rabbits for all stimulus intensities at 12 weeks of age (Fig. 3A). The intensity-response curve of the cone photoreceptors of the Tg rabbits overlapped that of the WT rabbits, indicating that the cone

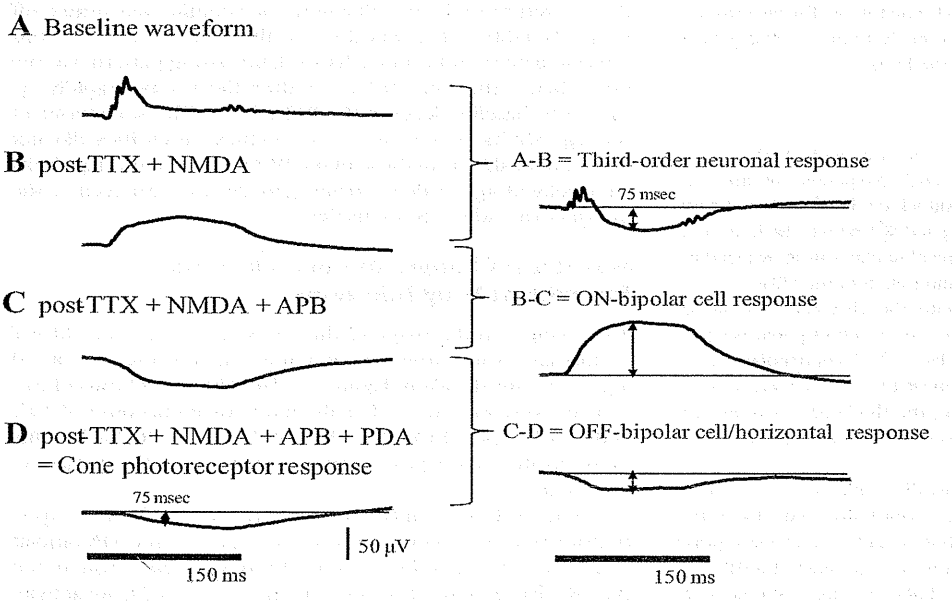

FIGURE 2. Baseline waveform (A) and waveform changes after intravitreal injection of TTX+NMDA alone (B) or with, APB (C), or APB+PDA (D). Averaged waveforms of ERGs elicited by 3.0 cd/m² from WT rabbits (n = 5) at 12 weeks of age. Digitally subtracted waveforms representing responses from the third-order neurons (A minus B: baseline minus post-TTX+NMDA), ON- bipolar cells (B minus C: post-TTX+NMDA minus post-TTX+NMDA+APB), and OFF-bipolar/horizontal cells (C minus D: post-TTX+NMDA+APB minus post-TTX+NMDA+APB+PDA). The amplitudes of each wave were measured at 75 ms after light onset.

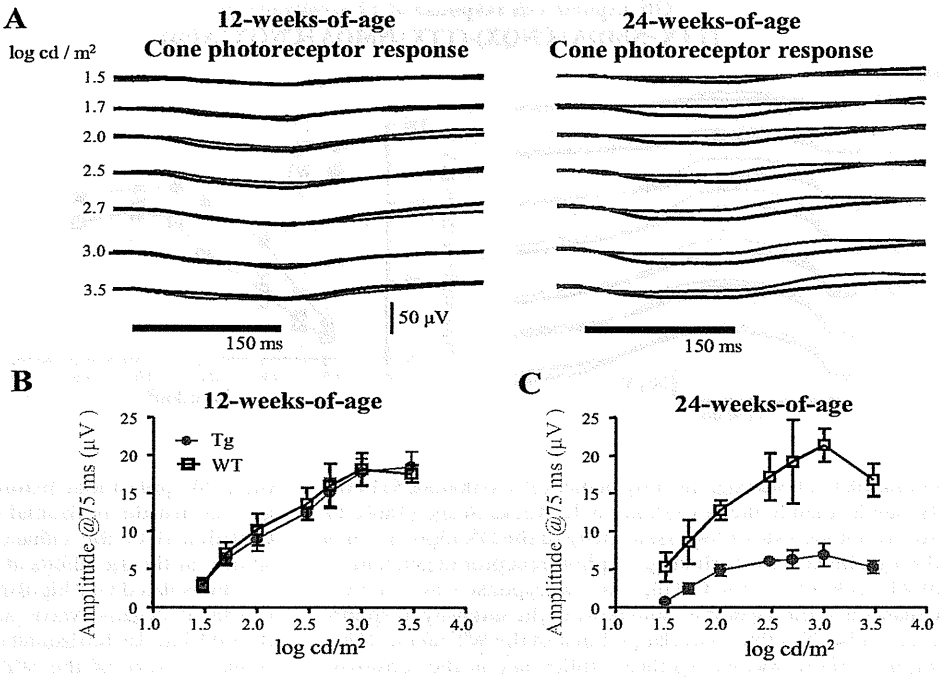

FIGURE 3. (A) Averaged waveforms of the cone photoreceptor responses from Pro347Leu Tg (n = 5) and WT (n = 5) rabbits at 12 and 24 weeks of age. *Black* and *red lines*: ERGs recorded from WT and Tg rabbits, respectively. The amplitudes of the cone photoreceptor responses are plotted against stimulus intensities for (B) 12- and (C) 24-week-old Tg and WT rabbits. Error bars, SD.

photoreceptor function remained unchanged in the Tg rabbits at this age (Fig. 3B). At 24 weeks of age, the averaged cone photoreceptor responses of Tg rabbits were less negative than those of WT rabbits (Fig. 3A). The curve of the Tg rabbits was significantly lower than that of the WT at all stimulus intensities ($P < 0.0001$), indicating a decrease in cone photoreceptor function (Fig. 3C).

The ON-bipolar cell response consisted of a slow, positive, trapezoid-shaped wave in both the Tg and WT rabbits. Interestingly, at 12 weeks of age, the averaged ON-bipolar cell responses of the Tg rabbits were more positive than those of the WT rabbits, especially at stimuli from 1.7 to 2.7 log cd/m^2 (Fig. 4A). The intensity–response curve of the ON-bipolar cells of the Tg rabbits was always significantly higher than that of WT rabbits, especially in the intermediate intensities from 1.7 to 2.7 log cd/m^2 (Fig. 4B; $P < 0.05$–0.001). The intensity–response curve of the Tg rabbits was significantly different from that of the WT rabbits ($P < 0.0001$). The sensitivity of the isolated ON-bipolar cell response was taken to be the stimulus intensity necessary to elicit one half of the maximum amplitude of the ON-bipolar cell response. From the intensity–response curve of each animal, the sensitivity of the ON-bipolar cell response was obtained and then averaged for the Tg and WT rabbits at 12 and 24 weeks of age. The sensitivity of the

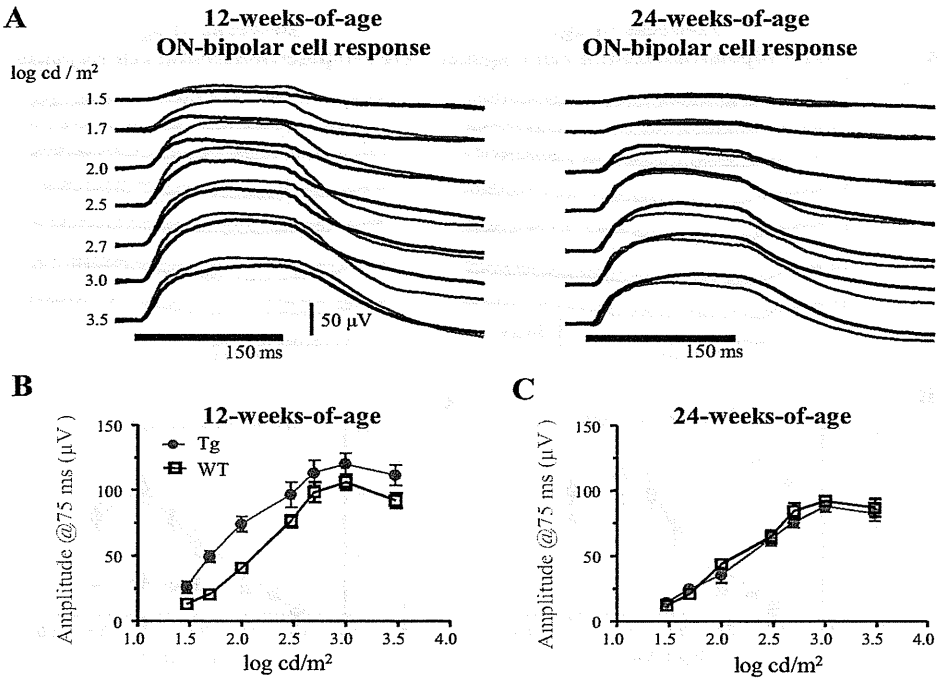

FIGURE 4. Averaged waveforms of the digitally subtracted response of the ON-bipolar cell recorded from Pro347Leu Tg (n = 5) and WT (n = 5) rabbits at 12 and 24 weeks of age (A). *Black* and *red lines*: ERGs recorded from WT and Tg rabbits, respectively. The amplitudes of the ON-bipolar cell responses are plotted against the stimulus intensities for (B) 12- and (C) 24-week-old Tg and WT rabbits. Error bars, SD.

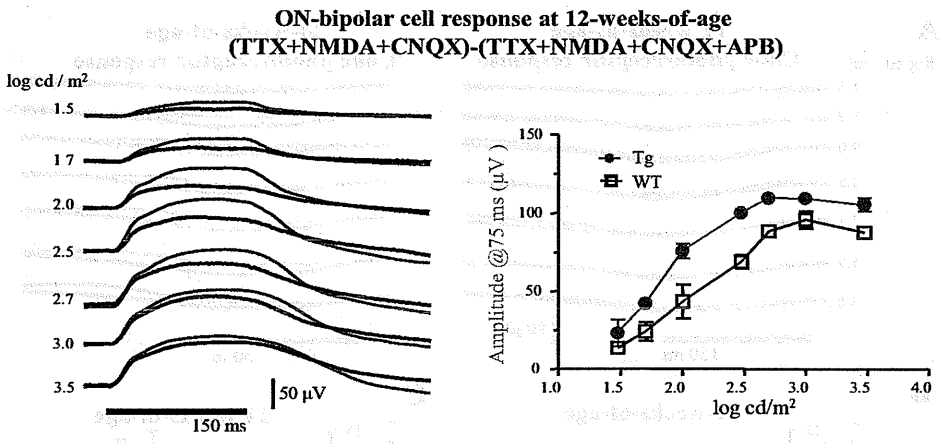

FIGURE 5. (A) Averaged ON-bipolar cell responses obtained by digitally subtracting the post-TTX+NMDA+CNQX+APB from the post-TTX+NMDA+CNQX *Black* and *red lines*: ERGs recorded from 12-week-old WT (n = 3) and Pro347Leu Tg (n = 3) rabbits, respectively. (B) The amplitudes of the ON-bipolar cell responses are plotted against the stimulus intensities for 12-week-old Tg and WT rabbits. Error bars, SD.

ON-bipolar cell was significantly higher ($P < 0.0000005$) in the Tg rabbits than in the WT rabbits at 12 weeks of age (Table 1). This result indicates a hypersensitivity of the ON-bipolar cell of the Tg rabbits at the early stage of photoreceptor degeneration. At 24 weeks of age, the ON-bipolar cell response was no longer enhanced in the Tg rabbits, and most of the intensity-response curve of the Tg rabbits overlapped that of the WT rabbits (Figs. 4A, 4C). There was no significant difference in the sensitivity between the Tg and WT animals at this age (Table 1).

The feedback from the horizontal cell to the cones could affect the ON-bipolar cell responses after APB was injected and before blocking the horizontal cell activity. After blocking the third-order neuronal activity by the TTX+NMDA injections, we injected CNQX before the APB injections in three Tg and WT rabbits at 12 weeks of age. Then, we isolated ON-bipolar cell responses without the contribution of the horizontal cell feedback by subtracting the post-TTX+NMDA+CNQX+APB from the post-TTX+NMDA+CNQX. The ON-bipolar cell responses of Tg rabbits were more positive than those of WT rabbits (Fig. 5A), and there was a significant difference in the intensity-response curves between Tg and WT rabbits (Fig. 5B; $P <$ 0 0001) These findings are identical with those obtained by the APB applications before the PDA injections (Fig. 4), suggesting that the horizontal cell feedback was unlikely to have contributed to the enhancement of the ON-bipolar cell response in the Tg rabbits at 12 weeks of age.

The isolated OFF-bipolar/horizontal cell response consisted of a small, negative wave. At 12 weeks of age, the waveform of the OFF-bipolar/horizontal cell responses of the Tg rabbits was similar to that of the WT rabbits (Fig. 6A). The intensity-response curve of the OFF-bipolar/horizontal cell response of the Tg rabbits overlapped that of the WT rabbits (Fig. 6B). At 24 weeks of age, the OFF-bipolar/horizontal responses of the Tg rabbits were significantly lower than those of the WT rabbits ($P < 0.0001$) at all stimulus intensities. The responses of the WT rabbits had a negative shape, with the amplitudes comparable to those at 12 weeks of age (Figs. 6A, 6C).

The third-order neuronal response consisted of a slow negative wave with oscillations corresponding to the onset and offset of the stimulus (Fig. 7A). At 12 weeks of age, the waveform in the Tg rabbits was more negative than that in the WT rabbits for stimuli from 1.5 to 2.5 log cd/m^2 (Fig. 7A). The amplitudes of the third-order neuronal responses were significantly larger in the Tg than in the WT rabbits from 1.5 to 2.0

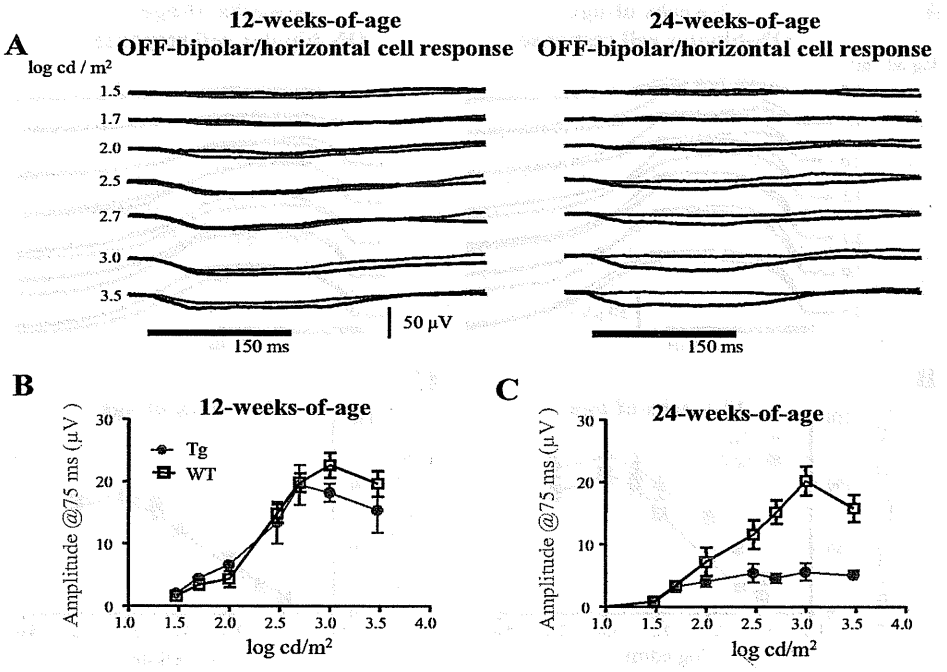

FIGURE 6. (A) Averaged waveforms of the digitally subtracted response of the OFF-bipolar/horizontal cell recorded from Pro347Leu Tg (n = 5) and WT (n = 5) rabbits at 12 and 24 weeks of age. *Black* and *red lines*: ERGs recorded from WT and Tg rabbits, respectively. The amplitudes of the OFF-bipolar/horizontal cell response are plotted against intensities of stimuli for (B) 12 and (C) 24-week-old Tg and WT rabbits Error bars, SD.

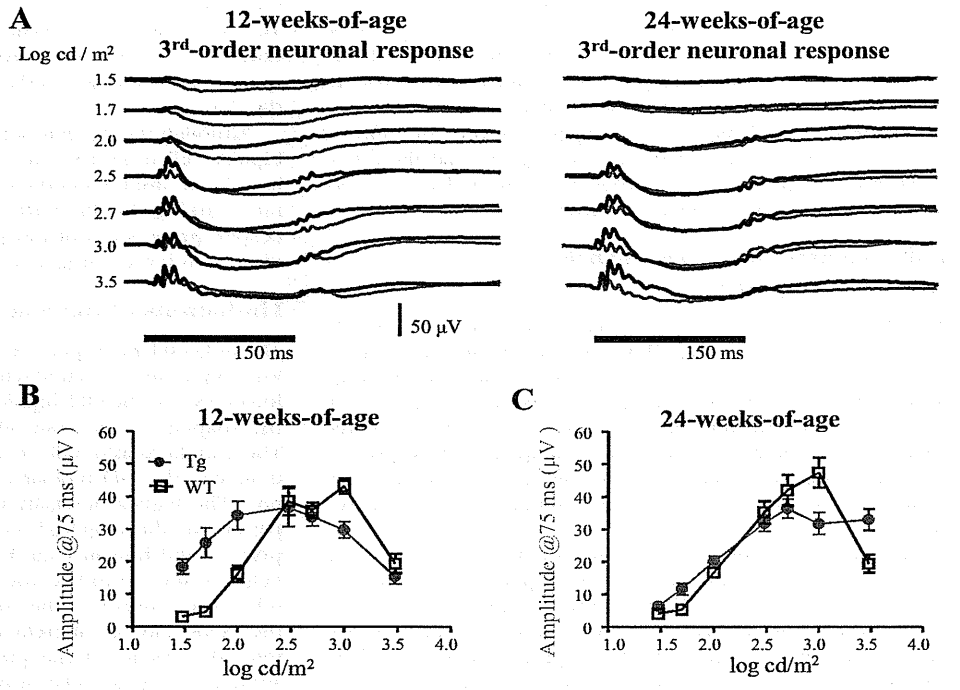

FIGURE 7. (A) Averaged waveforms of the digitally subtracted response of the third-order neurons recorded from Pro347Leu Tg ($n = 5$) and WT ($n = 5$) rabbits at 12 and 24 weeks of age. *Black* and *red lines*: ERGs recorded from WT and Tg rabbits, respectively. The amplitudes of the third-order neuronal response are plotted against the stimulus intensities for (B) 12- and (C) 24-week-old Tg and WT rabbits. Error bars, SD.

log cd/m^2 (Fig. 7B, $P < 0.001$). In 24-week-old Tg rabbits, oscillations elicited by ON stimuli were attenuated, but the slow negative response was not decreased (Figs. 7A, 7C).

DISCUSSION

Our results showed that the ERG component reflecting the ON-bipolar cell responses was enhanced at the early stage of photoreceptor degeneration in Pro347Leu Tg rabbits. In addition, the third-order neuronal responses were enhanced in the Tg rabbits. At a more advanced stage, the ON-bipolar and third-order neuronal responses were preserved despite functional loss of the cone photoreceptors and OFF-bipolar/horizontal cells. These results suggest that the light responses of neurons in the middle or inner retina were altered before the cone photoreceptors showed functional evidence of degeneration.

Depolarizing Pattern and Photoreceptor Degeneration

The presence of a depolarizing or a hyperpolarizing pattern of the cone ERG suggests abnormalities of signal transmission between the cone photoreceptor and the bipolar cell. Sieving et al.[17,18] termed the characteristic waveform of the cone ERGs elicited by long-duration stimuli a "depolarizing pattern," when the potential level after the b-wave does not return to the baseline level but remains elevated. Experimentally, ERGs with a depolarizing pattern have been recorded after the signals from the cones to the OFF-bipolar/horizontal cells are blocked by glutamate analogs, such as PDA and/or kynurenic acid (KYN).

Although experimental evidence has demonstrated that this unusual waveform is due to abnormalities of the synaptic transmission between the cone photoreceptors and the OFF-bipolar cells, a depolarizing pattern of the cone ERG has also been reported in human photoreceptor diseases. Sieving[29] reported a case of unilateral cone dystrophy with a depolarizing pattern of the cone ERG. Kondo and Miyake[30] reported a case of macular degeneration with a depolarizing pattern of the focal macular ERG. We also reported a case of age-related macular degeneration (AMD) that had a depolarizing pattern of the focal macular ERG after photodynamic therapy.[31] Common to these cases with a depolarizing pattern of the ERG was that the known abnormalities were mainly of the photoreceptors rather than the bipolar cell. The depolarizing pattern of the long-duration cone ERGs was seen in animal models with photoreceptor degeneration in the present study, adding further evidence that eyes with photoreceptor diseases can have a depolarizing pattern of the cone ERGs.

TABLE 1. Sensitivity of ON-Bipolar Cell Response

12 weeks of age		24 weeks of age	
Tg	WT	Tg	WT
1.85 ± 0 03	2 19 ± 0 03	2.16 ± 0.06	2 07 ± 0.06
$P < 0$ 0000005		NS	

Tabulated values give mean ± SD of intensity for 1/2 amplitude max(log cd/m^2).

Enhancement of ON-Bipolar Cell Responses

We found that the ON-bipolar cell responses, extracted by the use of APB, were enhanced for all the stimulus intensities at the early stage of degeneration when the rod photoreceptor degeneration had already begun.[11] This finding is consistent with our previous result in which the ON-bipolar cell response extracted from the mfERGs was enhanced in the Tg rabbits at the same age.[16] Because the cone photoreceptors and the OFF-bipolar/horizontal cell responses appeared to be nearly functionally normal at this stage, the loss of the rod photoreceptor may be involved in the enhancement of the ON-bipolar cell responses.

Similar findings have been made in rhodopsin-knockout mice[32,33] without rod outer segments as well as in neural retina leucine zipper (Nrl) knockout mice in which the rods fail to

develop and all photoreceptors are replaced by cones.[34] In both mouse models, the photopic cone b-wave amplitudes were larger than normal.[34–37] Because the contribution of the OFF-bipolar/horizontal cell response to the ERG is very small in mice, the enhancement of the cone b-wave indicates an augmentation of the ON-bipolar cell response of the cone ERGs. These findings support our results and suggest that the functional loss of rods could be a trigger for the enhanced ON-bipolar cell response of the cone ERGs.

Enhancement of the Third-Order Neuronal Response

The slow negative wave of the third-order neuronal response was enhanced at 12 weeks of age in the Tg rabbits and persisted at 24 weeks of age. The negative response most likely represents mainly the ON-photopic negative response (PhNR) which is driven by the ON pathway.[38] This finding corresponds to the enhancement of the ON-bipolar cell response, suggesting that enhancement of the ON-bipolar cell response contributes to the alterations in the third-order neuronal response.

Alternatively, there is evidence that the third-order neuronal responses are more preserved than the bipolar cell responses. We have shown that the NMDA-sensitive components of the cone ERGs are better preserved than the b-wave in RCS rats despite the progression of photoreceptor degeneration.[39] It has been reported that the TTX-sensitive components of the cone ERG are enhanced in Tg rabbits at the early stage.[12]

Synaptic Remodeling

Several immunohistologic studies of animal models with rod degeneration have demonstrated that the rod bipolar cells develop new synaptic connections with the functional cones after they lose their original connections to the rods because of rod degeneration.[10,40] This ectopic synaptic formation between surviving cones and rod bipolar cells may explain the significant enhancement or preservation of the ON-bipolar cell responses in Tg rabbits.

At 12 weeks of age, the loss of rod function had already started with a decrease in rod photoreceptors,[11] whereas cone photoreceptor function was normally preserved. Our hypothesis of synaptic remodeling can explain the enhancement of the ON-bipolar cell response in the Tg rabbits, although this hypothesis is based solely on functional data without any histopathologic evidence of synaptic remodeling in this model. In the normal state, the cone photoreceptors connect to ON- and OFF-bipolar cells, whereas the rod photoreceptors connect exclusively to ON-bipolar cells. After the rod photoreceptors start to degenerate, the rod bipolar cells receive signals from cones through newly developed synapses, which may contribute to shaping the ON-bipolar cell response of the cone ERGs, possibly leading to the enhancement of the ON-bipolar cell response.

In clinical cases of RP, Marc et al.[41] demonstrated a significant increase in the number of OFF-bipolar cells expressing functional ionotropic glutamate receptors (iGluR) in an RP patient who had surviving cones with shortened outer segments. They suggested that rod bipolar cells switched contacts to cones and expressed iGluR representing the functional characteristics of OFF-bipolar cells, which is not consistent with our ERG data. However, their patients had advanced RPs in contrast to the early stage of rod photoreceptor degeneration in our animals.

Increased Sensitivity of ON-Bipolar Cell Response

Although there was no difference in the maximum amplitude of the ON-bipolar cell responses between the Tg and the WT rabbits at 12 weeks, the ON-bipolar response was larger in the Tg than in the WT rabbits in the intermediate stimulus intensity range. As a result, the sensitivity of the ON-bipolar cell response was increased in the Tg rabbits compared with that in the WT.

Although the mechanism of the hypersensitivity of the ON-bipolar cell response remains undetermined, similar findings have been observed in the rod b-wave of rhodopsin transgenic rats carrying the Pro23His mutation.[42,43] In this rat model, despite progression of rod photoreceptor loss, the sensitivity of the rod b-wave was increased or maintained.

Limitations of the Study

The isolated OFF-response consisted of a slow negative wave of low amplitude compared with that of the monkey ERGs.[18] This indicates that the OFF-bipolar cell responses contribute less to the shaping of the cone ERGs in rabbits than in monkeys. These findings also indicate that the ON-bipolar cell responses dominate the OFF-bipolar cell response, even in normal rabbits. The highest intensity of stimuli produce a depolarizing pattern of the long-flash cone ERG in WT rabbits, whereas primate and human cone ERGs with high intensities show a negative waveform because of the photopic hill effect.[44] The relationship between the stimulus intensity and waveform of the rabbit ERG is different from that of human ERGs. Therefore, the results of the present study could not be simply applied to human ERGs in the diseased state.

A search of PubMed did not reveal any studies on RP cases with a depolarizing pattern of the cone ERG. On other hand, a hyperpolarizing pattern of the cone ERG and dysfunction of the ON-bipolar cell have been reported in RP patients.[45,46] The swine model with the Pro347Leu rhodopsin mutation showed abnormal development of the OFF-pathway.[47] These functional findings of the clinical cases and the swine model are not consistent with our results. The difference in species or in the stage of disease may have contributed to these discrepant findings.

Conclusions

A depolarizing pattern of the cone ERGs elicited by long-duration stimuli was seen in Pro347Leu Tg rabbits. The pharmacologic dissection of the cone ERG demonstrated that the enhancement or preservation of the ON-bipolar cell response contributed to shaping the specific waveforms in Tg rabbits. In this model, functional alterations of the ON-pathway took place before the cone photoreceptor function began to deteriorate.

References

1. Sung CH, Davenport CM, Hennessey JC, et al. Rhodopsin mutations in autosomal dominant retinitis pigmentosa. *Proc Natl Acad Sci USA.* 1991;88:6481–6485.
2. Sung CH, Schneider BG, Agarwal N, Papermaster DS, Nathans J. Functional heterogeneity of mutant rhodopsins responsible for autosomal dominant retinitis pigmentosa. *Proc Natl Acad Sci USA.* 1991;88.8840–8844.
3. Sung CH, Makino C, Baylor D, Nathans J. A rhodopsin gene mutation responsible for autosomal dominant retinitis pigmentosa results in a protein that is defective in localization to the photoreceptor outer segment. *J Neurosci.* 1994;14.5818–5833
4. Berson EL, Rosner B, Sandberg MA, et al. Ocular findings in patients with autosomal dominant retinitis pigmentosa and rhodopsin, proline-347-leucine. *Am J Ophthalmol.* 1991;111.614–623.
5. Oh KT, Longmuir R, Oh DM, et al. Comparison of the clinical expression of retinitis pigmentosa associated with rhodopsin mutations at codon 347 and codon 23. *Am J Ophthalmol.* 2003;136 306–313

6. Olsson JE, Gordon JW, Pawlyk BS, et al Transgenic mice with a rhodopsin mutation (Pro23His): a mouse model of autosomal dominant retinitis pigmentosa. *Neuron.* 1992;9 815–830
7. Naash MI, Hollyfield JG, Al-Ubaidi MR, Baehr W Simulation of human autosomal dominant retinitis pigmentosa in transgenic mice expressing a mutated murine opsin gene. *Proc Natl Acad Sci USA.* 1993;90:5499–5503.
8. Li T, Synder WK, Olsson JE, Dryja TP. Transgenic mice carrying the dominant rhodopsin mutation P347S: evidence for defective vectorial transport of rhodopsin to the outer segments. *Proc Natl Acad Sci USA.* 1996;93:14176–14181.
9. Green ES, Menz MD, LaVail MM, Flannery JG. Characterization of rhodopsin mis-sorting and constitutive activation in a transgenic rat model of retinitis pigmentosa. *Invest Ophthalmol Vis Sci.* 2000;41:1546–1553.
10. Peng YW, Hao Y, Petters RM, Wong F. Ectopic synaptogenesis in the mammalian retina caused by rod photoreceptor-specific mutations *Nat Neurosci.* 2000;3:1121–1127
11. Kondo M, Sakai T, Komeima K, et al. Generation of a transgenic rabbit model of retinal degeneration. *Invest Ophthalmol Vis Sci.* 2009;50 1371–1377
12. Sakai T, Kondo M, Ueno S, et al. Supernormal ERG oscillatory in transgenic rabbit with rhodopsin P347L mutation and retinal degeneration. *Invest Ophthalmol Vis Sci.* 2009;50 4402–4409.
13. Narahashi T, Moore JW, Scott WR Tetrodotoxin blockage of sodium conductance increase in lobster giant axons. *J Gen Physiol.* 1964;47:965–974.
14. Narahashi T. Chemicals as tools in the study of excitable membranes. *Physiol Rev.* 1974;54:813–889.
15. Bloomfield SA Effect of spike blockade on the receptive-field size of amacrine and ganglion cells in the rabbit retina *J Neurophysiol.* 1996,75.1878–1893
16. Yokoyama D, Machida S, Kondo M, et al. Pharmacological dissection of mulufocal electroretinograms of rabbits with Pro347L rhodopsin mutation. *Jpn J Ophthalmol.* 2010;54:458–466.
17. Sieving PA. Photopic ON- and OFF-pathway abnormalities in retinal dystrophies *Trans Am Ophthalmol Soc.* 1993,91:701–773.
18. Sieving PA, Murayama K, Naarendorp F. Push-pull model of the primate photopic electroretinogram: a role for hyperpolarizing neurons in shaping the b-wave. *Vis Neurosci.* 1994,11.519–532.
19. Kondo M, Piao CH, Tanikawa A, Horiguchi M, Miyake Y. A contact lens electrode with built-in high intensity white light-emitting diodes. *Doc Ophthalmol.* 2001;102:1–9.
20. Slaughter MM, Miller RF The role of excitatory amino acid transmitters in the mudpuppy retina. an analysis with kainic acid and N-methyl aspartate. *J Neurosci.* 1983;3:1701–1711.
21. Hood DC, Frishman LJ, Saszik S, Viswanathan S. Retinal origins of the primate multifocal ERG. implications for the human response. *Invest Ophthalmol Vis Sci.* 2002;43.1673–1685.
22. Slaughter MM, Miller RF. 2-Amino-4-phosphonobutyric acid a new pharmacological tool for retina research. *Science.* 1981;211 182–185
23. Slaughter MM, Miller RF. An excitatory amino acid antagonist blocks cone input to sign-conserving second-order retinal neuron. *Science.* 1983;219.1230–1232.
24. Bleakman D, Lodge D Neuropharmacology of AMPA and kinate receptors *Neuropharmacology.* 1998;37:1187–1204.
25. Mojumder DK, Sherry DM, Frishman LJ. Contribution of voltage-gated sodium channels to the b-wave of the mammalian flash electroretinogram *J Physiol.* 2008;586:2551–2580.
26. Gao H, Pennesi ME, QiaoX, et al. Intravitreal moxifloxacin. retinal safety study with electroretinography and histopathology in animal models. *Invest Ophthalmol Vis Sci.* 2006,47:1606–1611.
27. Horiguchi M, Suzuki S, Kondo M, et al Effect of glutamate analogues and inhibitory neurotransmitters on the electroretinograms elicited by random sequence stimuli in rabbits. *Invest Ophthalmol Vis Sci.* 1998;39:2171–2176.
28. Ng YF, Chan HH, Chu PH, et al. Multifocal electroretinogram in rhodopsin P347L transgenic pigs. *Invest Ophthalmol Vis Sci.* 2008, 49:2208–2215.
29. Sieving PA. Unilateral cone dystrophy: ERG changes implicate abnormal signaling by hyperpolarizing bipolar and/or horizontal cells. *Trans Am Ophthalmol Soc.* 1994;92.459–479.
30. Kondo M, Miyake Y. Assessment of local cone on- and off-pathway function using multifocal ERG technique. *Doc Ophthalmol.* 2000; 100:139–154.
31. Nishimura T, Machida S, Tamada K, Kurosaka D. Depolarizing focal macular electroretinogram pattern after photodynamic therapy in a patient with polypoidal choroidopathy. *Jpn J Ophthalmol.* 2010;54:509–511.
32. Humphries MM, Rancourt D, Farrar GJ, et al Retinopathy induced in mice by targeted disruption of the rhodopsin gene. *Nat Genet.* 1997;15.216–219.
33. Toda K, Bush RA, Humphries P, Sieving PA. The electroretinogram of the rhodopsin knockout mouse. *Vis Neurosci.* 1999;16 391–398
34. Mears AJ, Kondo M, Swain PK, et al. Nrl is required for rod photoreceptor development *Nat Genet.* 2001;29:447–452.
35. Jaissle GB, May CA, Reinhard J, et al Evaluation of the rhodopsin knockout mouse as a model of pure cone function. *Invest Ophthalmol Vis Sci.* 2001;42.506–513.
36. Haverkamp S, Michalakis S, Claes E, et al Synaptic plasticity in CNG3(−/−) mice: cone bipolar cell react on the missing cone input and form ectopic synapses with rods. *J Neurosci.* 2006,26: 5248–5255
37. Strettoi E, Mears AJ, Swaroop A Recruitment of the rod pathway by cones in the absence of rods. *J Neurosci.* 2004;24.7576–7582.
38. Viswanathan S, Frishman LJ, Robson JG, Harwerth RS, Smith EL 3rd. The photopic negative response of the macaque electroretinogram: reduction by experimental glaucoma. *Invest Ophthalmol Vis Sci.* 1999;40:1124–1136
39. Machida S, Raz-Prag D, Fariss RN, et al. Photopic ERG negative response from amacrine cell signaling in RCS rat retinal degeneration. *Invest Ophthalmol Vis Sci.* 2008;49:442–452.
40. Peng YW, Senda T, Hao Y, et al. Ectopic synaptogenesis during degeneration in the royal college of surgeons rat. *Neuroscience.* 2003;119:813–820.
41. Marc RE, Jones BW, Anderson JR, et al. Neural reprogramming in retinal degeneration. *Invest Ophthalmol Vis Sci.* 2007;48:3364–3371.
42. Machida S, Kondo M, Jamison JA, et al. P23H rhodopsin transgenic rat. correlation of retinal function with histopathology. *Invest Ophthalmol Vis Sci.* 2000;41:3200–3209.
43. Aleman TS, LaVail MM, Montemayor R, et al. Augmented rod bipolar cell function in partial receptor loss. an ERG study in P23H rhodopsin transgenic and aging normal rats. *Vision Res.* 2001;41: 2779–2797.
44. Ueno S, Kondo M, Niwa Y, Terasaki H, Miyake Y. Luminance dependence of neural components that underlies the primate photopic electroretinogram. *Invest Ophthalmol Vis Sci.* 2004;45: 1033–1040
45. Cideciyan AV, Jacobson SG. Negative electroretinograms in retinitis pigmentosa. *Invest Ophthalmol Vis Sci.* 1993;34:3253–3263.
46. Alexander KR, Barnes CS, Fishman GA. ON-pathway dysfunction and timing properties of the flicker ERG in carriers of X-linked retinitis pigmentosa. *Invest Ophthalmol Vis Sci.* 2003;44:4017–4025.
47. Banin E, Cideciyan AV, Aleman TS, et al. Retinal rod photoreceptor-specific gene mutation perturbs cone pathway development. *Neuron.* 1999;23:549–557.

Doc Ophthalmol (2011) 122:191–197
DOI 10.1007/s10633-011-9272-3

CASE REPORT

Melanoma-associated retinopathy associated with intranasal melanoma

Shigeki Machida · Hiroshi Ohguro · Masaru Tateda · Hiroaki Sato · Dajiro Kurosaka

Received: 31 March 2011 / Accepted: 19 April 2011 / Published online: 3 May 2011

Abstract
Purpose To present a case of melanoma-associated retinopathy (MAR) associated with an intranasal melanoma.
Case report A 77-year-old Japanese man visited us complaining of night blindness, blurred vision, and color vision difficulties in both eyes. His best-corrected visual acuity was 0.7 in the right and 1.0 in the left eyes. The rod response of the electroretinogram (ERG) was abolished, and the maximum response had a negative waveform. The a-wave of the single-flash cone response was square shaped, and the b-wave was delayed. The ON-response of the long-flash cone ERG was absent, but the OFF-response was preserved. A severe loss of retinal sensitivity was detected by static perimetry. Positron emission tomography showed no abnormal signs. Six months after the initial examination, an intranasal tumor was detected and surgically removed. The final diagnosis based on histopathology was malignant melanoma.
Conclusion Our case demonstrates that MAR can be associated with an intranasal mucosal melanoma. Thus, in cases where the primary lesion cannot be identified in patients with MAR-like symptoms and signs, we recommend that preferential sites of mucosal melanomas be examined.

Keywords Melanoma · Melanoma-associated retinopathy · Intranasal melanoma · Mucosal melanoma · Electroretinogram

S. Machida (✉) · D. Kurosaka
Department of Ophthalmology, Iwate Medical University School of Medicine, 19-1 Uchimaru, Morioka, Iwate 020-8505, Japan
e-mail: smachida@iwate-med.ac.jp

H. Ohguro
Department of Ophthalmology, Sapporo Medical University, School of Medicine, South-1 West-16 Chuo-ku, Sapporo, Hokkaido 060-8543, Japan

M. Tateda · H. Sato
Department of Otolaryngology, Iwate Medical University School of Medicine, 19-1 Uchimaru, Morioka, Iwate 020-8505, Japan

Introduction

The paraneoplastic syndromes are caused by autoimmune mechanisms associated with malignant tumors. Melanoma-associated retinopathy (MAR) is complicated by cutaneous malignant melanomas [1–3], and they are characterized by the loss of the function of ON-bipolar cells [4, 5]. Antibodies have been found in the sera against the bipolar cells of patients with MAR [6]. In addition, Lei et al. [7] demonstrated that an intravitreal injection of the sera obtained from MAR patients blocked the ON-bipolar response of the electroretinograms (ERGs) in monkeys. This suggested that antibodies circulating in the serum probably penetrated the blood–retinal barrier and altered the retinal function in patients diagnosed with

MAR. Most recently, it was reported that autoantibodies against TRPM1 cation channels of ON-bipolar cells were present in some MRA patients [8, 9].

The prevalence of malignant melanomas in highly pigmented individuals is less than onetenth of that of lightly pigmented individuals [10]. Therefore, MAR is very rare in the Japanese population, and only one case of MAR has been published in Japan [11]. In this case, the ERGs had the typical features of MAR but the primary lesion could not be found. The final diagnosis was made by histopathological findings of the metastatic lesion in the cervical lymph nodes. The results of this case suggested that a primary lesion other than a cutaneous melanoma may exist elsewhere.

Earlier MAR cases have been exclusively associated with cutaneous melanomas except for a few cases associated with a uveal melanoma [12–14]. We present a case of MAR associated with an intranasal melanoma that is a rare site and accounts for less than 1% of all malignant melanomas [15]. A search of PubMed did not extract any publication of MAR associated with a mucosal melanoma.

Case report

A 77-year-old Japanese man visited us in January 2008 complaining of metamorphopsia and decrease of vision in his right eye. His right eye had a macular hole, which was repaired by vitrectomy combined with cataract surgery. His symptoms disappeared with restoration of vision. He had skin carcinoma in 1998 and colon carcinoma in 2000, which were surgically removed. Otherwise, he had no medical history of any diseases.

He visited us in October 2009 complaining of an acute depression of night vision in the right eye that was followed by the same symptom in the left eye 2 weeks later. He also complained of blurred vision, photophobia in his right eye, and difficulty in discriminating blue from green. His best-corrected visual acuity (BCVA) had decreased from 1.0 to 0.7 in the right eye, but remained at 1.0 in his left eye. A mild invasion of inflammatory cells was found in the right vitreous. The ocular fundus appeared normal except for a slightly pale optic disc in the right eye (Fig. 1a and b). Spectral-domain optical coherence tomography (SD-OCT) of the left eye demonstrated normal structure and thickness of each retinal layer (Fig. 1c). The right eye had an abnormal configuration of the macula that had been repaired by the macular hole surgery.

We measured the critical flicker fusion frequency (CFF) by beginning with a high-frequency stimulus that the patient reported to be steady, i.e., fused. The frequency was slowly decreased until the patient reported that the stimulus appeared to be flickering. This frequency was taken as the critical fusion frequency. In this way, we determined that the CFF was abnormally reduced to 16 Hz in the left eye, but a flickering appearance was not detected at any frequency for the right eye.

Full-field ERGs were recorded using a contact lens electrodes carrying light-emitting diodes (LEDs: Mayo, Nagoya, Japan), which provided the white stimuli and background light. The luminance of the stimulus and background light at the corneal surface was measured with a photometer (Minolta LS-100, Minolta, Tokyo, Japan). The rod and maximum ERGs were elicited by white stimuli of luminances 0.48 and 3.3 log cd/m^2, respectively, with 3-ms stimulus duration. The cone ERGs were elicited by 3.0 log cd/m^2 stimuli of 3 ms duration, and the 30 Hz flicker ERGs were elicited by 2.0 log cd/m^2 stimuli. Both cone stimuli were presented on a white background of 40 cd/m^2. Long-duration cone ERGs were elicited by a stimulus of 150 ms duration and a luminance of 2.5 log cd/m^2 on the same background. In addition, we recorded focal macular ERGs elicited by a 15 degree stimulus spot with duration of 100 ms. The stimulus and background intensities were 160 and 6.9 cd/m^2, respectively.

In October 2009, the rod ERGs were extinguished, and the maximal response had a negative waveform (arrows in Fig. 2). The single-flash cone response had a square-shaped a-wave (asterisk) and a reduced b-wave amplitude and prolonged implicit time. The amplitudes of the 30 Hz flicker ERGs were normal but delayed. These ERG findings were compatible with a loss of the ON-response [16].

The cone responses elicited by long-duration stimuli showed a loss of the ON-response but preservation of the OFF response (Fig. 3). The focal macular ERG also showed a loss of the ON-response with preservation of the OFF-response. These ERG findings are not only consistent with those of complete type of congenital stationary blindness

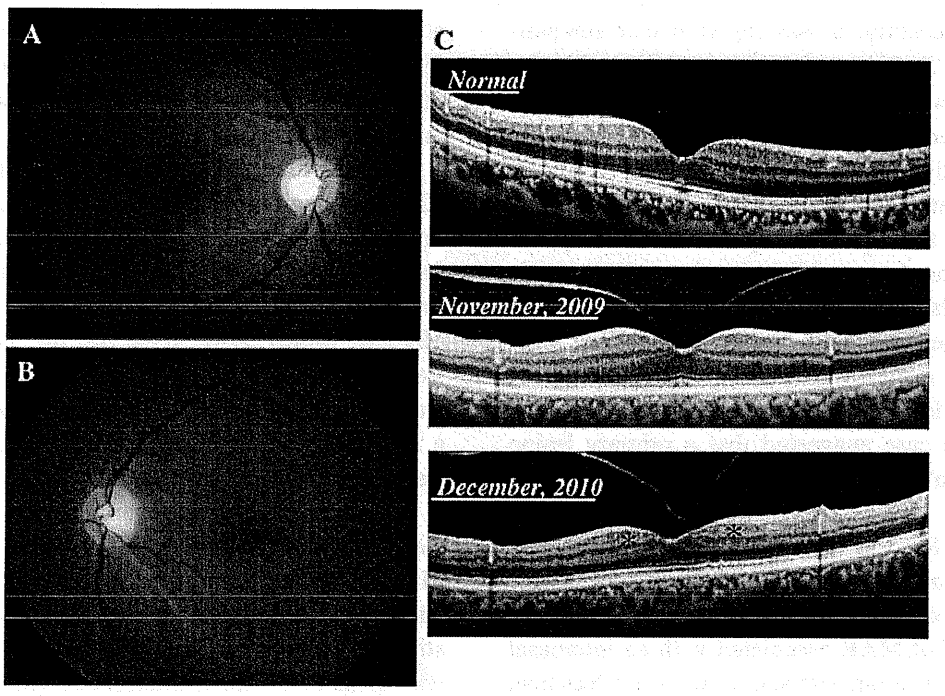

Fig. 1 Fundus photographs and spectral-domain optical coherence tomographic (SD-OCT) image of a patient with melanoma-associated retinopathy (MAR). **a** and **b** Fundi appeared normal except for a slightly pale optic nerve head in the right eye. **c** SD-OCT of our MAR patient and an age-matched normal subject. In December 2010, the inner retina of the paramacula became thinner compared to the baseline (November 2009) or the normal subject (indicated by *asterisks*)

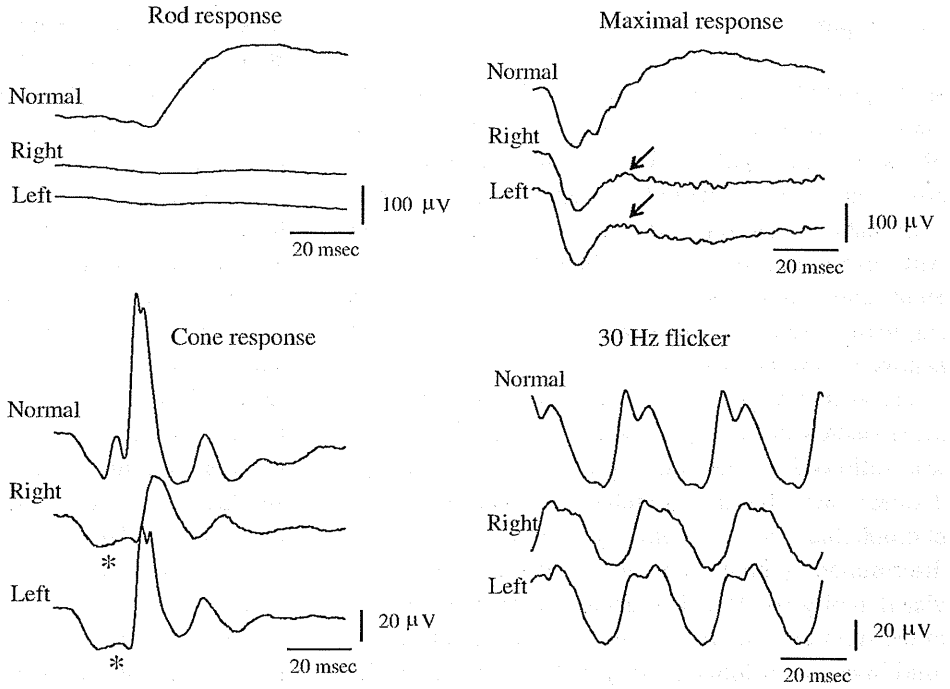

Fig. 2 Full-field standard electroretinograms (ERGs) recorded from an age-matched normal subject and our MAR patient including rod, maximal, cone, and 30 Hz flicker responses. *Arrows* in the maximal response indicate reduced b-wave amplitude with a shape of the negative ERGs. *Asterisks* indicate square-shaped a-waves of the cone ERG

(cCSNB) in humans and in monkeys treated with an intravitreal injection of 2-amino-4-phosphonobutyric acid (APB) [17] but also with those of MAR.

Static perimetry demonstrated severe loss of the visual sensitivity, and the mean deviation was less than −30 dB for both eyes (Fig. 4a). Kinetic

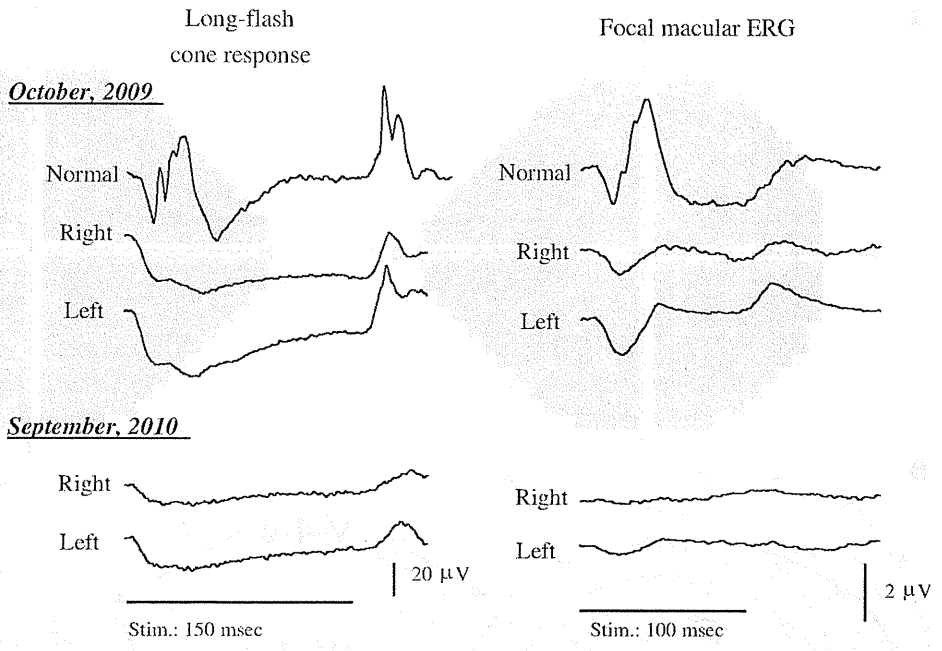

Fig. 3 Long-duration cone electroretinogram (ERG) and focal macular ERGs demonstrate the selective loss of the ON-response in October 2009. The OFF-response was also attenuated in September 2010

perimetry, however, showed a relative preservation of the peripheral visual field with central and paracentral scotomas (Fig. 4b).

Because we suspected MAR based on the ERG findings, we consulted a dermatologist who did not find any signs of a cutaneous melanoma. Whole-body computed tomography (CT) and positron emission tomography (PET) showed no signs of a malignant tumor in December 2009 (Fig. 5a). The patient visited the Department of Otolaryngology because of a feeling of left nasal obstruction in April 2010. PET-CT demonstrated ^{18}F-fluorodeoxy glucose (FDG) accumulation in the left nasal cavity in May 2010 (Fig. 5b). MRI revealed a tumor occupying the left nasal cavity (Fig. 5c).

In June 2010, the tumor was surgically removed. Histopathology showed features compatible with a malignant melanoma, including a pigmented lesion composed of diffusely distributed cells within the submucosal layer. The neoplastic cells had round to spindle-shaped nuclei with dense chromatin and heavily pigmented cytoplasma. A final diagnosis of malignant melanoma was made by positive immunohistological staining for HMB-45 and S-100.

Sera from our MAR patient and a normal subject were evaluated by immunocytochemistry. Immunofluorescence was performed on cryostat sections of unfixed rat retinas. Heavy immunostaining was seen in the inner nuclear and inner plexiform layers with weak staining in the ganglion cell layer in the MAR patient, while no staining was detected in the normal control (Fig. 5d).

ERGs were recorded again in September 2010, 11 months after the visual symptom began. The long-flash cone and focal macular ERGs demonstrated a loss of the ON- and OFF-responses (Fig. 3). At the final visit in December 2010, the BCVA was 0.01 in the right and 0.03 in the left eye. SD-OCT demonstrated a thinning of the inner plexiform and ganglion cell layers in the paramacular regions of the left eye (asterisks, Fig. 1c). A regional recurrence and metastasis were not found at the final visit.

Discussion

MAR associated with mucosal melanoma

To the best of our knowledge, this is the first case of MAR associated with a mucosal melanoma. Mucosal melanomas preferentially affect mucosa of the nasal cavity, paranasal sinuses, oropharynx, anus/rectum, vagina, and urinary tract [10]. Mucosal melanomas are more prevalent in lightly pigmented than heavily pigmented individuals. However, in African–American and Hispanic individuals, there is a higher percentage of mucosal melanoma out of all melanomas than in white individuals (12.2% vs 1.3%). This

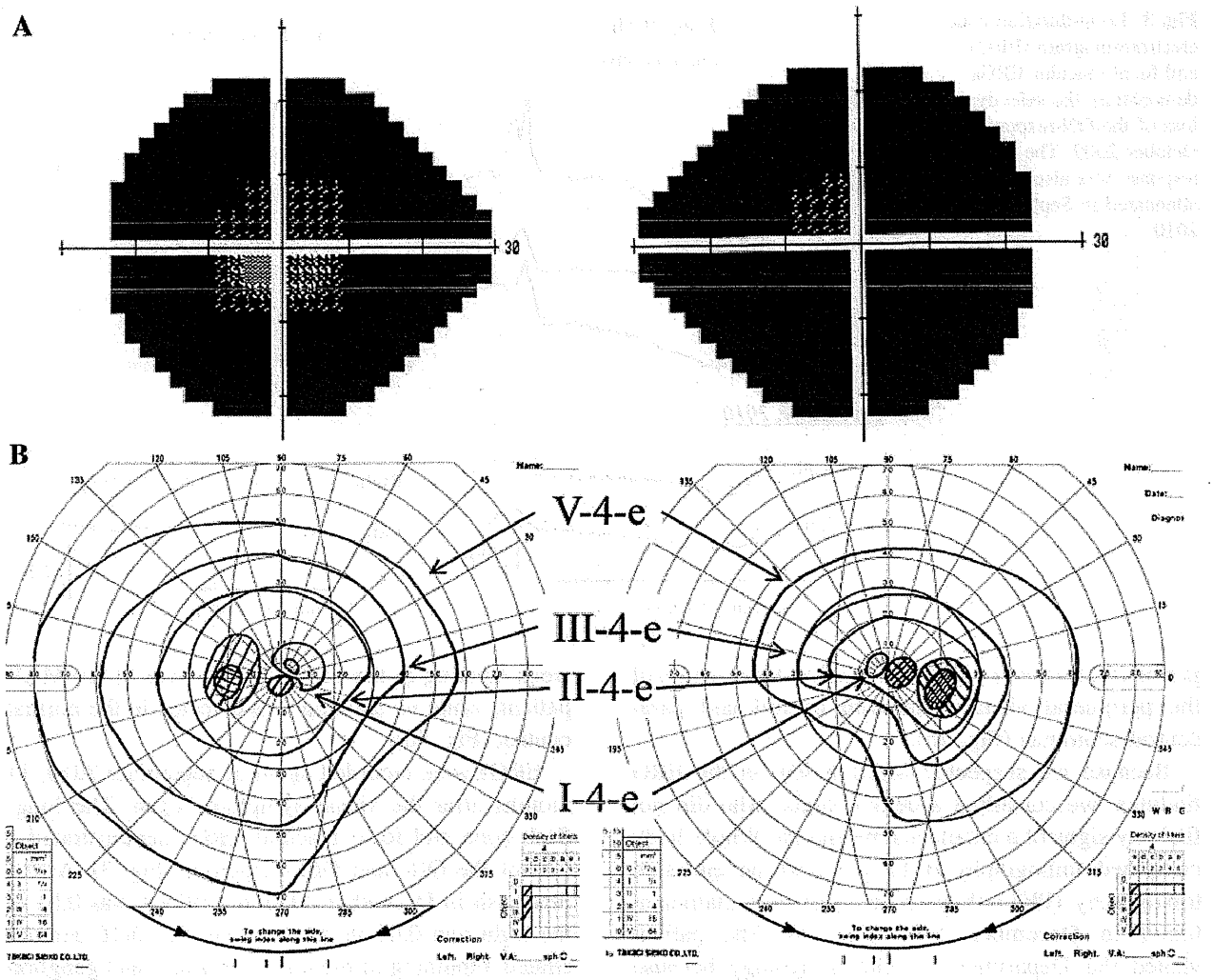

Fig. 4 Perimetric findings in our patient with MAR. **a** Static perimetry. **b** Kinetic perimetry

would indicate that the relative incidence of mucosal melanoma is high in highly pigmented individuals. Thus, a mucosal melanoma should be considered to be the primary site of MAR in pigmented individuals.

In most patients with MAR complicated by cutaneous melanoma, the primary lesions were easily identified because the skin lesions usually preceded the onset of MAR. The symptoms associated with an intranasal melanoma are nonspecific, so that it is difficult to make an early diagnosis. The first PET image appeared normal and failed to identify the primary lesion. Therefore, we recommend that mucosal sites be examined more extensively for mucosal melanomas if the electrophysiological test shows the typical features of MAR.

Discrepancies between visual tests

Interestingly, the visual function measured by the static perimetry was severely altered in our case in contrast to being normal in cCSNB patients in which the ERG findings are identical to MAR [18]. In the sera of the previous MAR patients, several kinds of antibodies were identified, indicating that retinal elements other than the ON-bipolar cells [14] may be involved in the pathophysiology of MAR. In our case, light staining was seen in the retinal ganglion cell layer, suggesting the retinal ganglion cells were also impaired, which could explain the difference in the visual function between MAR and cCSNB.

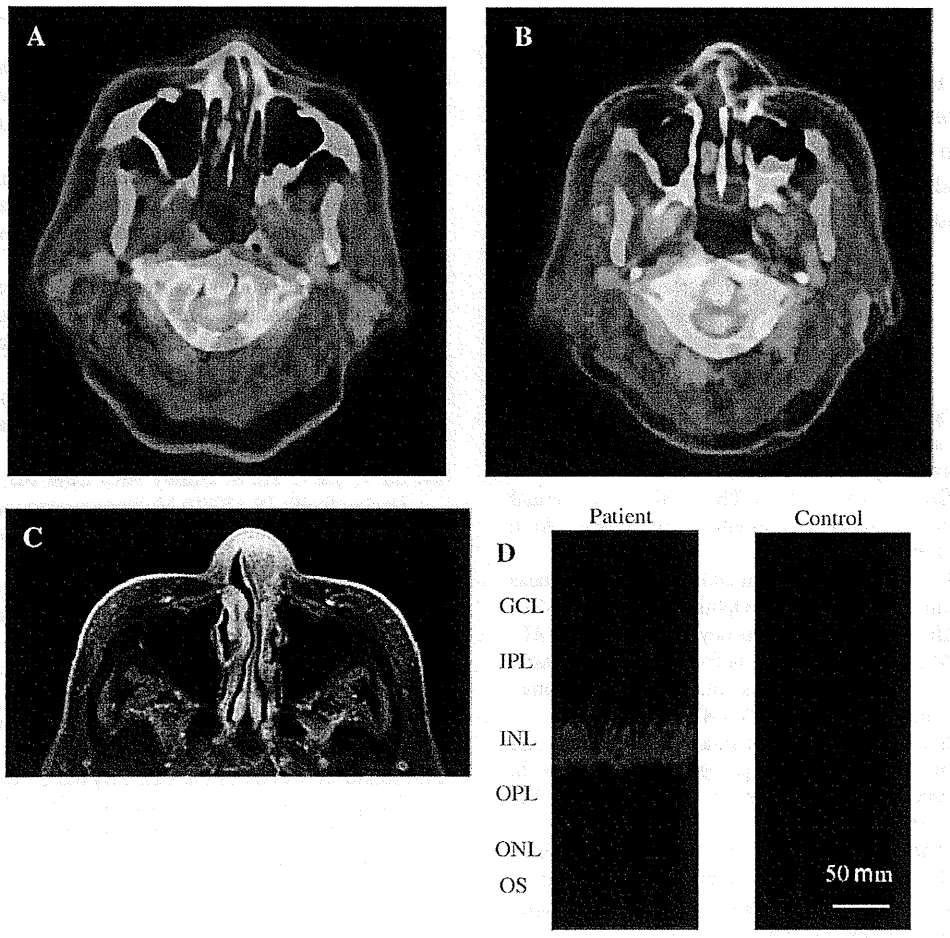

Fig. 5 **a** Positron emission tomography (PET)–computed tomography (CT) could not find abnormal signs in December 2009. **b** PET-CT showed abnormal accumulation of ^{8}F-fluorodeoxy glucose in the left nasal cavity in May 2010. **c** A tumor in the left nasal cavity was identified by MRI in May 2010. **d** Immunofluorescence was performed on cryostat sections of unfixed rat retinas. *GCL* ganglion cell layer, *IPL* inner plexiform layer, *INL* inner nuclear layer, *OPL* outer plexiform layer, *ONL* outer nuclear layer, *OS* outer segment

Wolf and Arden found severe deficits in the temporal contrast sensitivity in MAR patients, whereas the spatial contrast sensitivity was relatively well preserved at high spatial frequencies [19]. They concluded that there is a selective loss of function of the magnocellular pathway with functional preservation of the parvocellular pathway in MAR patients. This could account for our finding that the CFF was severely impaired despite good visual acuity.

SD-OCT findings in MAR

Recent advances of imaging the retina have enabled us to evaluate the morphology of each retinal layer in vivo. SD-OCT of our patient demonstrated normal structure and thickness of each retinal layer at the early stage of disease. However, progressive thinning of the inner retina of the paramacular region was seen 1 year after the visual symptoms began. These results suggest that functional loss precedes the anatomical loss of the retina in MAR.

A histopathological study of postmortem retinas of a MAR patient revealed no anatomic abnormalities throughout the retina by light microscopy [20]. In contrast to these findings, other histopathological study of MAR patients showed marked reduction in the density of bipolar cells with preservation of photoreceptor cells [21]. The large variations in the retinal histology of MAR patients may be because of differences in the stage of the disease.

Conclusions

Our findings indicate that MAR can be associated with a mucosal melanoma. In cases where the primary lesion cannot be detected in MAR patients, we recommend examining sites that are preferentially affected by mucosal melanomas.

References

1. Ripps H, Carr RE, Siegel IM, Greenstein VC (1984) Functional abnormalities in vincristine-induced night blindness. Invest Ophthalmol Vis Sci 25:787–794
2. DuBois L, Sadum AA, Lawton TB (1988) Inner retinal layer loss in complicated migraine. Case report. Arch Ophthalmol 106:1035–1037
3. Berson EL, Lessell S (1988) Paraneoplastic night blindness with malignant melanoma. Am J Ophthalmol 106:307–311
4. Alexander KR, Fishman GA, Peachey NS, Marchese AL, Tso MO (1992) 'On' response defect in paraneoplastic night blindness with cutaneous malignant melanoma. Invest Ophthalmol Vis Sci 33:477–483
5. Alexander KR, Barnes CS, Fishman GA, Milam AH (2002) Nature of the cone ON-pathyway dysfunction in melanoma-associated retinopathy. Invest Ophthalmol Vis Sci 43:1189–1197
6. Milam AH, Saari JC, Jacobson SG, Lubinski WP, Feun LG, Alexander KR (1993) Autoantibodies against retinal bipolar cells in cutaneous melanoma-associated retinopathy. Invest Ophthalmol Vis Sci 34:91–100
7. Lei B, Bush RA, Milam AH, Sieving PA (2000) Human melanoma-associated retinopathy (MAR) antibodies alter the retinal ON-response of the monkey ERG in vivo. Invest Ophthalmol Vis Sci 41:262–266
8. Dhingra A, Fina ME, Neinstein A, Ramsey DJ, Xu Y, Fishman GA, Alexander KR, Qian H, Peachey NS, Gregg RG, Vardi N (2011) Autoantibodies in melanoma-associated retinopathy target TRPM1 cation channels of retinal ON bipolar cells. J Neurosci 31:3962–3967
9. Kondo M, Sanuki R, Ueno S, Nishizawa Y, Hashimoto N, Ohguro H, Yamamoto S, Machida S, Terasaki H, Adamus G, Furukawa T (2011) Identification of autoantibodies against TRPM1 in patients with paraneoplastic retinopathy associated with ON bipolar cell dysfunction. PloS One (in press)
10. Chang AE, Karnell LH, Menck HR (1998) The national cancer data base report on cutaneous and noncutaneous melanoma. A summary of 84, 836 cases from past decade. Cancer 83:1664–1678
11. Murayama K, Takita H, Kiyohara Y, Shimizu Y, Tsuchida T, Yoneya S (2006) Melanoma-associated retinopathy with unknown primary site in a Japanese woman. Nippon Ganka Gakkai Zasshi 110:211–217
12. Zacks DN, Pinnolis MK, Berson EL, Gragoudas ES (2001) Melanoma-associated retinopathy and recurrent exudative retinal detachments in a patient with choroidal melanoma. Am J Ophthalmol 132:578–581
13. Nieuwenddijk TJ, Hooymans JM (2007) Paraneoplastic vitelliform retinopathy associated with meastatic choroidal melanoma. Eye 21:1436–1437
14. Lu Y, Jia L, He S, Hurley MC, Leys MJ, Jayasundera T, Heckenlively JR (2009) Melanoma-associated retinopathy. A paraneoplastic autoimmune complication. Arch Ophthalmol 127:1572–1580
15. Khanna R, Srivastava RN, Agarwal A (1990) Primary malignant melanoma of the nasal cavity. Ear Nose Throat J 69:654–655
16. Kondo M, Sieving PA (2001) Primate photopic sinewave flicker ERG: vector modeling analysis of component origins using glutamate analogs. Invest Ophthalmol Vis Sci 42:305–312
17. Kondo M, Ueno S, Piao CH, Miyake Y, Terasaki H (2008) Comparison of focal macular cone ERGs in complete-type congenital stationary night blindness and APB-treated monkeys. Vision Res 48:273–280
18. Terasaki H, Miyake Y, Nomura R, Horiguchi M, Suzuki S, Kondo M (1999) Blue-on-yellow perimetry in the complete type of congenital stationary night blindness. Invest Ophthalmol Vis Sci 40:2761–2764
19. Wolf JE, Arden GB (1996) Selective magnocellular damage in melanoma-associated retinopathy: comparison with congenital stationary nightblindness. Vision Res. 36:2369–2379
20. Keltner JL, Thirkill CE, Yip PY (2001) Clinical and immunologic characteristics of melanoma-associated retinopathy syndrome: eleven new cases and a review of 51 previously published cases. J Neuroophthalmol 21:173–187
21. Gittinger JW Jr, Smith TW (1999) Cutaneous melanoma-associated paraneoplastic retinopathy: histopathologic observations. Am J Ophthalmol 127:612–614